Snap buckling of a confined thin elastic sheet

G. Napoli[1] and S. Turzi[2]

[1]Dipartimento di Ingegneria dell'Innovazione, Università del Salento, via per Monteroni, Edificio 'Corpo O', Lecce 73100, Italy

[2]Dipartimento di Matematica, Politecnico di Milano, Piazza Leonardo da Vinci 32, Milano 20132, Italy

Received: 29 June 2015

Accepted: 27 October 2015

Author for correspondence:

G. Napoli

e-mail: gaetano.napoli@unisalento.it

1. Introduction

Elastic strips and rods are fundamental physical structures that can be found in many contexts on many different length scales. Often, they appear in the theoretical description of physical phenomena where the interplay between physics and geometry plays a key role. The collapse of an elastic sheet adhered to a curved substrate is certainly one of them. This discontinuous buckling instability appears in various problems in biology (shapes and morphogenesis of the mitochondrion [1]), physics (packing of thin films [2], delamination of thin elastic films [3,4], design of stretchable electronic devices [5], buckling of colloidal droplets [6], elastocapillary snapping [7]) and engineering (collapse of buried steel pipelines [8,9]).

A simple example illustrates the physical phenomenon we are concerned with. Let us imagine inserting a rectangular piece of paper inside a rigid cylindrical substrate. We hold the two edges with the hands so that the sheet of paper is kept in contact with the cylinder. Subsequently, we apply an increasing tangential

compressive force. Because of the presence of the surrounding container, the sheet of paper cannot freely deform to the outside. Initially, it appears to be undeformed or slightly compressed. However, when the applied force crosses a suitable threshold, the strip abruptly buckles and forms an inward hump. What is the critical force at which the collapse occurs? How are the geometric features of the hump at the transition related to the material constants and to the geometry of the container? Although the buckling of slender elastic structures is one of the oldest fundamental problems, nobody seems to have addressed these points. Furthermore, it is worth noticing that classical bifurcation analysis fails in this situation due to the confinement.

The simplified approach described here might provide a first model suited to explore the mechanical instabilities in many different contexts. For example, many living structures are coated by thin films, which have distinct mechanical properties from the substrate. These thin layers may grow faster or slower than the inner core. The interplay between tension and compression plays a critical role in enhancing the structural rigidity of certain plants [10]. In the human brain, recent studies show that the differential growth might be responsible for cortical folding [11]. A non-biological application is reported in [12], where the appearance of voids in a layered material confined to a V-shaped corner is attributed to the combined effect of bending stiffness, overburden pressure and geometric constraints. Another related problem deals with the packing of a flexible cylinder inside a rigid circular tube of smaller radius. This is widely explored in the literature, both theoretically [13] and experimentally [2]. Recent papers have also included the possibility of adherence by capillarity [14,15] or the extension to the spherical geometry [16].

In the usual theoretical treatment, the strip is modelled as an inextensible Euler beam, whose energy is only associated with the bending mode. The inextensibility assumption, first suggested by Rayleigh [17], is based on energetic considerations. The bending energy and the stretching energy scale differently with the beam thickness. When the structure thickness is diminished without limit, stretching is energetically prohibitively expensive and the distortion is pure bending. However, the validity of this assumption is challenged when the thickness becomes comparable to some other length scales in the problem. Moreover, axial compressibility is known to change the nature of the phase transition. For example, the usual supercritical bifurcation point in the classical inextensible Euler beam becomes a subcritical bifurcation [18,19]. In confined problems, the effect of finite compressibility on buckling has been studied by a number of authors [20–22] using the Föppl–von Kármán model.

However in our confined problem, the assumption of an axially inextensible beam shows its inadequacy in a more fundamental way. For instance, in the limit of an arbitrarily small hump, the inextensible Euler elastica model predicts the unphysical result of an infinite pressure exerted by the beam on the external container [13,14]. This prevents the transition to a buckled state as it would require an infinite force to induce buckling.

To avoid this unacceptable behaviour, in this paper, we revise this effect by allowing the sheet to both stretch and bend. Within this framework, the energy landscape exhibits a first-order phase transition from a state where compression energy dominates to another where bending energy prevails. From the mechanical point of view, a *snap through* buckling occurs: as the sheet grows, it suddenly switches from a completely adhered solution to a buckled solution showing a symmetric inward hump. The transition is studied numerically and, in the limit of *weak stretchability*, we provide the analytic expressions for the main quantities at the critical point. Interestingly, we find that for homogeneous beams, the threshold does not depend on the material parameters but only on the geometric features of the problem.

The paper is organized as follows. In §2, we derive the equilibrium equations from the theory of stretchable Kirchhoff's rods. The proper mathematical formulation of the model requires the introduction of two global geometrical constraints due to the unilateral confinement. We find two kinds of equilibrium solutions: the completely adhered solution and the collapsed (or buckled) solution. In §3, we perform a numerical simulation of the equilibrium stored energy for different solutions. The collapsed solution shows a bifurcation point (a cusp) and two branches. We prove that for small displacements of the endpoints, the completely adhered solution is energetically favoured; by contrast, the collapsed solution attains the energy minimum beyond a critical

displacement. We also provide an asymptotic approximation of the critical parameters at the transition. Section 4 is devoted to the analysis of the local stability of the buckled solution. We study the sign of the second variation of the energy functional. A first analysis based on Poincaré's inequality allows us to roughly estimate the region of stability, while a more precise picture is obtained by a conjugate-point analysis. In §5, we reach the conclusion and add some final comments. A variational formulation of the problem, including the mathematical details of the first and the second variation of the energy functional, is given in Appendix A.

2. The model

We assume a planar configuration so that the longitudinal profile of the strip can be modelled as a stretchable and flexible rod. This is represented by a parametric curve $\mathbf{r}(S)$, with $S \in [-L/2, L/2]$, where L denotes the length of the strip in the stress-free configuration and S is the referential arclength. The governing nonlinear Kirchhoff equations express the balance of linear and angular momentum. When an external distributed force $\mathbf{f}$ is applied and in absence of external distributed torques, they read

$$\mathbf{T}' + \mathbf{f} = \mathbf{0} \tag{2.1}$$

and

$$\mathbf{M}' + \mathbf{r}' \times \mathbf{T} = \mathbf{0}, \tag{2.2}$$

where $\mathbf{T}(S)$ and $\mathbf{M}(S)$ represent the internal forces and the internal torques, respectively. The prime denotes differentiation with respect to S; hence, $\mathbf{r}' = \lambda \mathbf{t}$, where λ is the local stretch and $\mathbf{t}$ is the unit tangent. The inextensibility condition corresponds to $\lambda = 1$.

Balance equations are complemented by the linear constitutive laws [23]:

$$\mathbf{T} = b(\lambda - 1)\mathbf{t} + T_n \mathbf{n} \tag{2.3}$$

and

$$\mathbf{M} = k\mathbf{t} \times \mathbf{t}', \tag{2.4}$$

where the positive constants b and k represent the stretching and the bending rigidity, respectively. The quantity $\ell = \sqrt{k/b}$ defines an intrinsic characteristic length. Since $b = EA$ and $k = EI$, where E is the elastic modulus of the material, A is the area of the film cross-section and I is the second moment of area of the strip cross-section, the intrinsic length ℓ turns out to be of the order of the strip thickness. Only the tension is given constitutively; the shear internal force T_n is related to the derivative of the internal torque by equation (2.2). We parametrize the tangent and the normal unit vectors by

$$\mathbf{t} = \cos\theta(S)\mathbf{e}_x + \sin\theta(S)\mathbf{e}_y \quad \text{and} \quad \mathbf{n} = -\sin\theta(S)\mathbf{e}_x + \cos\theta(S)\mathbf{e}_y$$

and, hence, $\mathbf{e}_z = \mathbf{t} \times \mathbf{n}$. Consequently, equation (2.4) reduces to $\mathbf{M} = k\theta'\mathbf{e}_z$.

Furthermore, we posit a symmetric equilibrium configuration of the rod and assume that the *displacement* of its endpoints can be controlled: the point with referential coordinate $S = L/2$ undergoes a tangential compressive displacement $r\Delta\alpha$, $\Delta\alpha \geq 0$. The strip can both stretch and bend, therefore there are at least two equilibrium configurations with the same imposed $\Delta\alpha$: (i) the *adhered solution* where the strip, uniformly compressed, totally adheres to the wall, and (ii) the *collapsed solution* with an inward symmetric hump. The adhered solution is a uniformly compressed arc of circumference with

$$\lambda_{\text{adh}} = 1 - \frac{2r\Delta\alpha}{L} \quad \text{and} \quad \theta'_{\text{adh}} = -\frac{\lambda_{\text{adh}}}{r}.$$

On the other hand, the collapsed solution comprises two parts: a free (non-adhered) curve for $S \in (-\bar{S}, \bar{S})$ and two adhered pieces for $S \in [-L/2, -\bar{S}] \cup [\bar{S}, L/2]$ (figure 1). The symmetry of the strip implies that the function $\theta(S)$ is odd and allows us to restrict the study of the solution in the range $S \in [0, L/2]$.

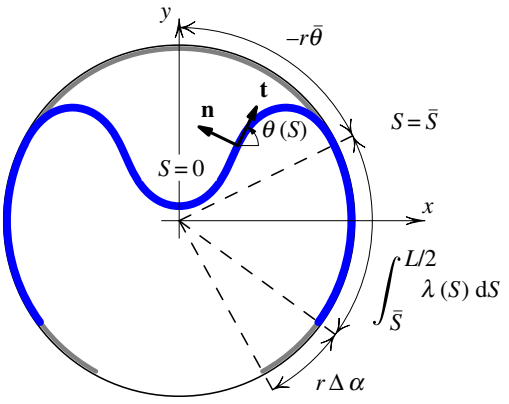

Figure 1. Schematic of the strip deformation. The grey curve represents the referential configuration, while the blue curve shows the buckled configuration with a hump due to the displacement $r\Delta\alpha$ of the endpoints. (Online version in colour.)

Since the adhered part, $S \in [\bar{S}, L/2]$, is an arc of circumference with $\theta'(S) = -\lambda/r$, the internal torque is $\mathbf{M} = -k(\lambda/r)\mathbf{e}_z$. Therefore, the equilibrium equations for this imposed geometry necessarily give $T_n = 0$ and $\lambda' = 0$, whence $\lambda(S) = \bar{\lambda} = \text{const}$. However, the compressive tangential force $\mathbf{F} = -F\mathbf{t}$ for a given $\Delta\alpha$ is not known *a priori* but it is related to the stretch by $F = b(1-\bar{\lambda})$.

In the non-adhered region, $S \in [0, \bar{S}]$, there is no applied distributed load ($\mathbf{f} = \mathbf{0}$). Furthermore, since $\theta(S)$ is odd, the vertical component of the tension vanishes, while the horizontal component, denoted by T_x, is constant and satisfies the equation

$$b(\lambda - 1) = T_x \cos\theta. \tag{2.5}$$

The balance of the torque yields the second-order differential equation for the free part

$$\theta'' + \lambda\tau \sin\theta = 0, \tag{2.6}$$

where $\tau = -T_x/k$.

The deflection angle $\theta(S)$ should satisfy the Dirichlet boundary conditions $\theta(0) = 0, \theta(\bar{S}) = \bar{\theta}$. Further boundary conditions are provided by requiring the continuity of the tangential component of the internal force and the continuity of the torque at the detachment point $S = \bar{S}$. These yield

$$T_x \cos\bar{\theta} = -b(1-\bar{\lambda}) \tag{2.7}$$

and

$$\theta'(\bar{S}) = -\bar{\lambda} r^{-1}, \tag{2.8}$$

respectively. One more constraint translates the geometrical condition that the detachment point must lie on the circumference of radius r

$$\int_0^{\bar{S}} \lambda \cos\theta \,\mathrm{d}S = -r\sin\bar{\theta}. \tag{2.9}$$

On the other hand, the displacement of the endpoint, $r\Delta\alpha$, is related to $\bar{\lambda}$, $\bar{S}$ and $\bar{\theta}$ by (figure 1)

$$r\Delta\alpha = r\bar{\theta} + (1-\bar{\lambda})\frac{L}{2} + \bar{\lambda}\bar{S}. \tag{2.10}$$

This geometrical identity is simply obtained by requiring that the total length is the sum of the hump length and the adhered length.

3. Results

We start by observing that for a perfectly unstretchable strip, the compression modulus diverges and the intrinsic length vanishes, $\ell = 0$. The tangential component of the internal force, T_t, then becomes a Lagrange multiplier associated with the inextensibility constraint $\lambda = 1$ and the adhered solution is admissible only for $\Delta\alpha = 0$.

By contrast, when both compression and bending are allowed, the energy must attain its absolute minimum in the observed solution, either adhered or collapsed, which is then expected to be stable. The other possible solution is either non-existing, unstable or metastable, depending on the energy landscape. The total elastic energy consists of two terms, related, respectively, to the bending mode and to the stretching (or compression) mode:

$$W = \frac{k}{2}\int_{-L/2}^{L/2} (\theta')^2 \, \mathrm{d}S + \frac{b}{2}\int_{-L/2}^{L/2} (1-\lambda)^2 \, \mathrm{d}S. \tag{3.1}$$

Equation (3.1) assumes a particularly simple analytic form when evaluated in the adhered solution

$$W_{\mathrm{adh}} = \frac{1}{2}\frac{kL}{r^2} + 2\frac{k}{r}\Delta\alpha\left[-1 + \frac{r}{L}(1+\xi^{-2})\Delta\alpha\right], \tag{3.2}$$

where $\xi = \ell/r > 0$ measures the compressibility strength at fixed radius.

On the other hand, the energy associated with the collapsed solution, W_{col}, is not amenable for a simple analytical approximation and is best calculated with a numerical simulation. Figure 2 shows the comparison between the energies associated with each branch as a function of $\Delta\alpha$, for fixed $\xi = 0.01$. The adhered branch depends quadratically on $\Delta\alpha$ (equation (3.2)). The collapsed solution comprises two branches. The upper branch, with higher energy, corresponds to small humps, whereas the lower branch corresponds to equilibrium solutions with larger humps. Finally, it is worth noticing that for sufficiently small values of $\Delta\alpha$ only the adhered solution is admissible.

Figure 2 clearly shows the first-order transition that occurs between the two solutions. For small displacements of the endpoints, the adhered solution is energetically favoured. However, when the displacement crosses a critical value $r(\Delta\alpha)_{\mathrm{cr}}$, the energy attains its absolute minimum at the collapsed solution *with a larger hump*. Therefore, as $\Delta\alpha$ is increased, the strip undergoes a discontinuous transition, abruptly passing from an adhered configuration to a buckled solution with an inward hump. The presence of compressibility implies a lower bound for the hump size: humps whose dimensions are small compared to the characteristic length ℓ cannot be observed and the strip is simply compressed. The critical threshold increases as the strip becomes softer (figure 3). In particular, in the inextensible limit, the critical threshold vanishes as expected.

In the *nearly unstretchable* regime ($\xi \ll 1$), one can estimate the critical threshold analytically. Indeed, at low ξ and close to the critical point, it has been observed numerically that the collapsed solution is nearly equivalent to the buckled profile of a perfectly inextensible strip. Figure 2 clearly shows this agreement in terms of elastic energies. From the analytic approximation, we also learn that the relevant variable for scaling the critical threshold is the *reduced compressibility*, defined as

$$\xi_0 := \xi\sqrt{\frac{L}{2r}}.$$

This indicates an unexpected non-trivial dependence on the geometrical and material parameters. For homogeneous materials, ξ_0 is just a geometrical dimensionless parameter, since both the compression and the bending rigidity are linear functions of the Young modulus. By contrast, the material moduli could play a role in the case of composite materials where the dependence of b and k on the Young modulus is more complex.

When the compression modulus is large ($\xi \ll 1$), compression becomes energetically prohibitively expensive for small $\Delta\alpha$. The strip then prefers to buckle and pay some bending energy provided it can relax its compression energy. Therefore, it is natural to approximate the collapsed strip as inextensible. The advantage of this approximation is that it is now possible

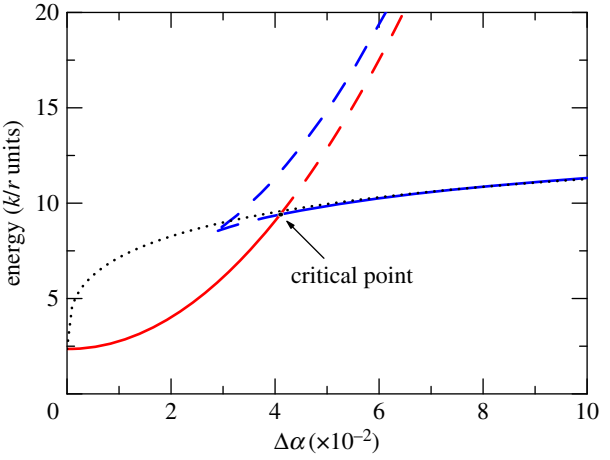

Figure 2. Plot of the equilibrium free energy W for the adhered solution (red) and the collapsed solution (blue) with $L = \frac{3}{2}\pi r$ and $\xi = 0.01$. Solid lines represent solutions with least energy; dashed lines represent metastable states or maxima. For small $\Delta\alpha$, only the adhered solution is admissible. The dotted line represents the energy of a perfectly inextensible strip as given in equation (3.10). (Online version in colour.)

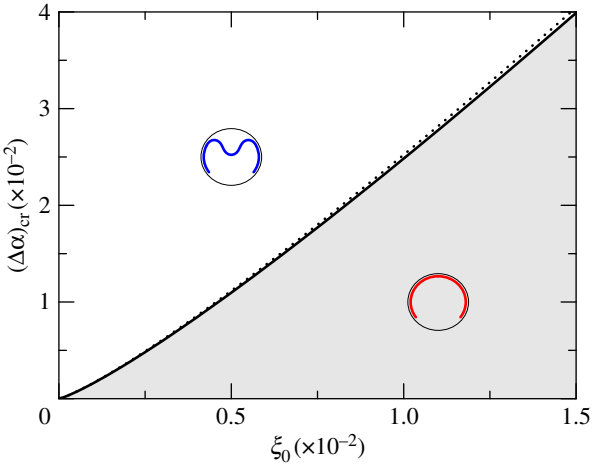

Figure 3. Critical threshold $(\Delta\alpha)_{cr}$ as a function of the reduced compressibility. The solid line represents the numerical results, while the dotted line represents the analytical approximate result as given in equation (3.11). Typical shapes are shown in the inset. (Online version in colour.)

to perform an analytic treatment. In particular, equation (2.6) simply reduces to the nonlinear pendulum equation with first integral

$$(\theta')^2 = 2\tau(\cos\theta - \cos\theta_0), \tag{3.3}$$

where $\theta_0 = \theta(S_0) \in [0, \pi]$ is the maximum value of $\theta(S)$ in $(0, \bar{S})$. The boundary condition for θ' at $\bar{S}$ becomes $\theta'(\bar{S}) = -1/r$. This is used together with the first integral to eliminate τ in favour of θ_0. Thus, we arrive at the first-order differential equation

$$\theta' = \pm\frac{1}{r}\sqrt{\frac{\cos\theta - \cos\theta_0}{\cos\bar{\theta} - \cos\theta_0}}, \tag{3.4}$$

where the sign + (respectively, −) is to be used in the interval $S \in (0, S_0)$ (respectively, $S \in (S_0, \bar{S})$). By symmetry, $\theta(0) = 0$ and equation (3.4) evaluated at $S = 0$ shows that $\cos\bar{\theta} - \cos\theta_0 > 0$. This gives a restriction on the possible values of $\bar{\theta}$: $|\bar{\theta}| < \theta_0$. Furthermore, equation (3.4) is an ordinary differential equation which can be solved by separation of variables in $(0, \bar{S})$ ([14, §3])

$$2\mathrm{F}(q_0) - \mathrm{F}(\bar{q}) = \frac{\bar{S}}{2r}\sqrt{\frac{1-\cos\theta_0}{\cos\bar{\theta} - \cos\theta_0}}, \tag{3.5}$$

where F denotes the incomplete elliptic integral of first kind [24] and, for ease of notation, we set

$$q_0 := \left\{\frac{\theta_0}{2}, \csc^2\left(\frac{\theta_0}{2}\right)\right\} \quad \text{and} \quad \bar{q} := \left\{\frac{\bar{\theta}}{2}, \csc^2\left(\frac{\theta_0}{2}\right)\right\}.$$

Similarly, we simplify equation (2.9) (with $\lambda = 1$) as follows:

$$2\mathrm{E}(q_0) - \mathrm{E}(\bar{q}) = -\frac{\bar{S}\cos\theta_0 + r\sin\bar{\theta}}{2r(1-\cos\theta_0)}\sqrt{\frac{1-\cos\theta_0}{\cos\bar{\theta} - \cos\theta_0}}, \tag{3.6}$$

where E represents the incomplete elliptic integral of second kind. Equations (3.5), (3.6) and the inextensible version of equation (2.10), $r\Delta\alpha = r\bar{\theta} + \bar{S}$, provide $\bar{S}$, θ_0 and $\bar{\theta}$ as functions of $\Delta\alpha$. In the limit $\Delta\alpha \ll 1$, after some tedious but straightforward calculations which we omit for brevity, it is possible to find the asymptotic expansions of θ_0 and $\bar{\theta}$ [14]

$$\theta_0 \approx 2.3454(\Delta\alpha)^{1/3} - 0.78762\Delta\alpha + 0.68361(\Delta\alpha)^{5/3} \tag{3.7}$$

and

$$\bar{\theta} \approx -2.2894(\Delta\alpha)^{1/3} + 0.83072\Delta\alpha - 0.62489(\Delta\alpha)^{5/3}. \tag{3.8}$$

The energy of an inextensible buckled solution has a particularly simple expression when it is written in terms of θ_0, $\bar{\theta}$ and $\bar{S}$. To this end, we insert equations (3.4), (2.9) and $\lambda = 1$ into equation (3.1) to get

$$\begin{aligned} W_{\mathrm{col}} &= k\int_0^{\bar{S}} (\theta')^2 \mathrm{d}S + k\int_{\bar{S}}^{L/2} (\theta')^2 \mathrm{d}S = \frac{k}{r^2}\int_0^{\bar{S}} \frac{\cos\theta(S) - \cos\theta_0}{\cos\bar{\theta} - \cos\theta_0}\mathrm{d}S + \frac{k}{r^2}\left(\frac{L}{2} - \bar{S}\right) \\ &= \frac{1}{2}\frac{kL}{r^2} - \frac{k}{r^2}\frac{\bar{S}\cos\bar{\theta} + r\sin\bar{\theta}}{\cos\bar{\theta} - \cos\theta_0}. \end{aligned} \tag{3.9}$$

The asymptotic expansions of θ_0 and $\bar{\theta}$ are then inserted into equation (3.9) to yield the approximate expression for the energy of the collapsed solution

$$W_{\mathrm{col}} \approx \frac{1}{2}\frac{kL}{r^2} + \frac{k}{r}(w_0(\Delta\alpha)^{1/3} + w_1\Delta\alpha + w_2(\Delta\alpha)^{5/3}), \tag{3.10}$$

where $w_0 \approx 23.113, w_1 \approx -18.532$ and $w_2 \approx 1.6131$. Thus, we are able to give an approximate analytic solution of the transition equation $W_{\mathrm{col}} = W_{\mathrm{adh}}$, which to leading order reads

$$(\Delta\alpha)_{\mathrm{cr}} \approx 6.5813\xi_0^{6/5}. \tag{3.11}$$

As shown in figure 3, this expression provides a very good account of the numerical results, in the range of compressibility considered.

Figure 4 sketches the critical behaviour of the detachment angle. This angle is directly related to the hump dimension and is easily accessible experimentally. For a given ξ, $|\bar{\theta}_{\mathrm{cr}}|$ represents the minimum stable detachment angle. Lower values of $\bar{\theta}$ corresponds to metastable or unstable solution. Thus, we can conclude that there is a limiting size below which the hump cannot develop. The dotted line in figure 4 represents the asymptotic approximation $|\bar{\theta}_{\mathrm{cr}}| \approx 4.29\,\xi_0^{2/5}$.

The lower bound for the blister size corresponds to a higher bound for the applied tangential force and thus for the pressure exerted on the delimiting container. Figure 5 reports the behaviour

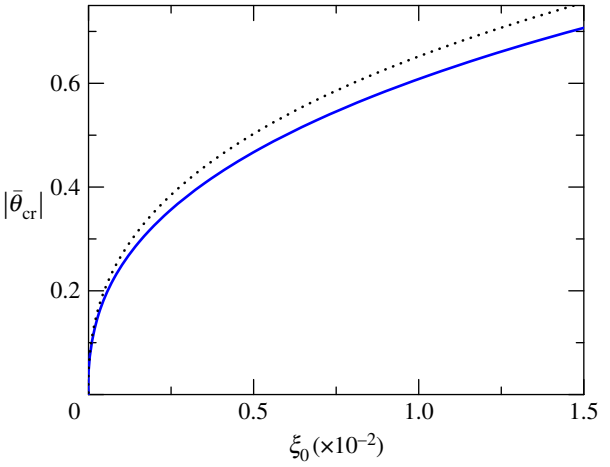

Figure 4. Detachment angle at the transition as a function of ξ. The dotted line represents the asymptotic approximation. (Online version in colour.)

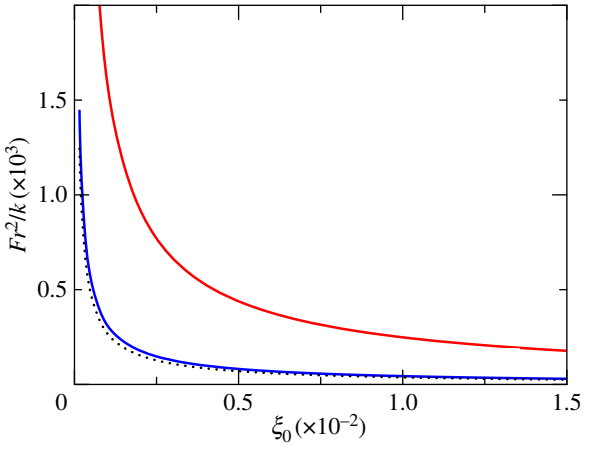

Figure 5. Tangential compressive force at the transition in the adhered solution (red line) and collapsed solution (blue line) as a function of ξ. The tangential force has a finite jump at the transition. The dotted lines show the asymptotic approximations. (Online version in colour.)

at the transition of the tangential force for the adhered (red line) and collapsed (blue line) solutions, as functions of the reduced compressibility. Since at the transition the solution passes from one to the other, the tangential force undergoes a discontinuous jump. This is consistent with the idea of buckling as the mechanism through which the system relaxes its internal stress. For fixed ξ_0, the correspondent value of the red line shows the maximum internal force acceptable by the system under pure compression. The critical load at which the buckling occurs is given by $F_{cr} = 2br(\Delta\alpha)_{cr}/L$. Furthermore, when $\Delta\alpha$ is below its critical threshold, the internal force is simply proportional to the strain and hence it vanishes as $\Delta\alpha$ tends to zero.

4. Local stability

We now consider the local stability of the equilibrium solutions in more detail. The second variation of the stored energy functional is calculated in the appendix and it is reported here

below for ease of reading

$$\delta^2 W = 2k \int_0^{\bar{S}} \left[h'^2 - \tau h(\lambda^* \cos\theta^* h + 2 \sin\theta^* u) + \frac{u^2}{r^2 \xi^2} \right] \mathrm{d}S, \tag{4.1}$$

where $\theta^*(S)$ and $\lambda^*(S)$ are the equilibrium solutions, $h(S)$, $u(S)$ are their small perturbations and $\xi^2 = k/(br^2)$. Standard results in the calculus of variations [25,26] show that the positive definiteness of the second variation is a necessary condition for the stability and a sufficient condition for the existence of a weak minimum of the total energy. For a given $h(S)$, the minimum of the integrand (and thus that of $\delta^2 W$) is achieved when $u(S)$ is a stationary value: $u(S) = \tau r^2 \xi^2 h(S) \sin\theta^*(S)$. Therefore, if $\delta^2 W$ is positive for this $u(S)$ we know that it is positive for all other possible variations. On the other hand, if $\delta^2 W$ is negative for this $u(S)$ there may be some $u(S)$ which make the second variation positive, but nevertheless we have been able to show that the second variation is not always positive and the equilibrium is unstable. This allows us to simplify the problem and consider the *reduced* second variation in the sole variable $h(S)$

$$\delta^2 W^{(r)} = 2k \int_0^{\bar{S}} [h'^2 - \tau(\cos\theta^* - r^2 \xi^2 \tau \cos(2\theta^*)) h^2] \, \mathrm{d}S. \tag{4.2}$$

Taking into account the boundary conditions $h(0) = 0$ and $h(\bar{S}) = 0$ for admissible variations, we can use the Poincaré inequality

$$\int_0^{\bar{S}} h'^2 \mathrm{d}S \geq \frac{\pi^2}{\bar{S}^2} \int_0^{\bar{S}} h^2 \, \mathrm{d}S, \tag{4.3}$$

to find a lower bound for the second variation

$$\begin{aligned} \delta^2 W^{(r)} &\geq 2k \int_0^{\bar{S}} \left[\frac{\pi^2}{\bar{S}^2} - \tau \cos\theta^* + r^2 \xi^2 \tau^2 \cos(2\theta^*) \right] h^2 \, \mathrm{d}S \\ &\geq 2k \int_0^{\bar{S}} \left[\frac{\pi^2}{\bar{S}^2} - \tau(1 + r^2 \xi^2 \tau) \right] h^2 \, \mathrm{d}S. \end{aligned} \tag{4.4}$$

Hence, the second variation is positive-definite, and the equilibrium is stable, provided that the compressive force is limited by

$$\tau(1 + r^2 \xi^2 \tau) \bar{S}^2 < \pi^2. \tag{4.5}$$

It is worth remarking at this point that the lower branch of the buckled solution in figure 2 corresponds to nearly uncompressed states (and therefore τ is generally small). By contrast, the highly compressed states (high τ) are represented by the upper branch. Equation (4.5) thus suggests that the lower branch is stable, while the upper branch is unstable.

(a) Conjugate-point analysis

To get a more precise picture of the stability and to show that the above crude analysis is indeed qualitatively correct, we now study the Jacobi accessory problem associated to (4.2). We refer to the standard literature on the calculus of variations for details (e.g. [25,26]). The presence of the global (or 'isoperimetric' in the calculus of variations parlance) constraint (2.9) introduces some mathematical subtleties into the formulation of the accessory equation (see [27,28] for a fuller discussion). The key point is that the second variation has to be positive with respect to all variations *tangent* to the constraint. In our case, the *linearized* constraint is derived in appendix (equation (A 10)). Its reduced form is

$$\int_0^{\bar{S}} (1 - 2r^2 \xi^2 \tau \cos\theta^*) \sin\theta^* h \, \mathrm{d}S = 0, \tag{4.6}$$

and this poses a global restriction on the admissible variations $h(S)$.

We say that $S=\sigma$ is a *isoperimetric conjugate point* to $S=0$ if there exist a constant κ and a function $h(S)$ not identically zero which are solution to the following system ($0 \le S \le \sigma$):

$$\left.\begin{aligned} &h'' + \tau(\cos\theta^* - r^2\xi^2\tau\cos(2\theta^*))h = \kappa(1 - 2r^2\xi^2\tau\cos\theta^*)\sin\theta^*, \\ &h(0) = h(\sigma) = 0 \\ \text{and}\quad &\int_0^\sigma (1 - 2r^2\xi^2\tau\cos\theta^*)\sin\theta^* h\,\mathrm{d}S = 0. \end{aligned}\right\} \tag{4.7}$$

The homogeneous differential equation associated to the ODE in (4.7) is simply the Euler–Lagrange equation of the functional (4.2) with respect to $h(S)$. Standard theorems in the classical calculus of variations say that the energy has a weak minimum (and the equilibrium is stable) if there is no point conjugate to $S=0$ in $(0,\bar{S}]$; there is a bifurcation point if $\sigma=\bar{S}$ (and the equilibrium is unstable); finally when $\sigma<\bar{S}$, the equilibrium is unstable.

The linearization of (4.7) suffices to correctly capture the main features of the problem, as can be checked numerically, and at the same time provides neat analytical results on the bifurcation condition. To this end, we use the fact that the linearized equilibrium solution is $\theta^*(S) = A\sin(\omega S)$, with A a suitable constant, and approximate (4.7) with

$$\left.\begin{aligned} &h'' + \omega^2 h = \kappa\sin(\omega S), \quad \omega = \sqrt{\tau(1 - r^2\xi^2\tau)}, \\ &h(0) = h(\sigma) = 0 \\ \text{and}\quad &\int_0^\sigma \sin(\omega S)h(S)\,\mathrm{d}S = 0, \end{aligned}\right\} \tag{4.8}$$

where on the right-hand side all the constants have been absorbed into κ. The solution to this problem is easily found to be

$$h(S) = C\left(\sin(\omega S) + 2\omega S\cos(2\omega S)\frac{2\omega\sigma - \sin(2\omega\sigma)}{2\omega\sigma\cos(2\omega\sigma) - \sin(2\omega\sigma)}\right), \tag{4.9}$$

with C an arbitrary integration constant. The condition $h(\sigma)=0$ yields an equation for $\omega\sigma$ which is solved numerically to give

$$\omega\sigma \approx 4.60. \tag{4.10}$$

The bifurcation point, and thus the critical stress τ_c, is obtained by imposing $\sigma=\bar{S}$ as the conjugate point. Specifically, we have the following equation for τ_c

$$(\omega_c\bar{S})^2 = \tau_c(1 - r^2\xi^2\tau_c)\bar{S}^2 \approx (4.60)^2, \tag{4.11}$$

which shows a remarkable agreement with the numerical simulation: the numerical value obtained at the cusp point of figure 2 is $\omega_c\bar{S} \approx 4.57$. The solution is unstable if $\sigma<\bar{S}$ and this corresponds to $\omega = \omega_c\bar{S}/\sigma > \omega_c$, i.e. $\tau > \tau_c$. Finally, when $\tau<\tau_c$, the solution is stable.

5. Concluding remarks

In many applied contexts, it is useful to study the slightly different problem where the sheet is closed, i.e. the lateral ends of the strip are glued together. For instance, the elastic sheet can be made of a growing biological membrane confined by a rigid cylinder of radius r. In this case, the circumferential growth, suitably measured by $\epsilon := (L - 2\pi r)/(2\pi r)$, may trigger the instability. For moderate growth, the excess material can simply result in a uniform compression of the adhered strip and in an increase of the hoop stress. By contrast, a further increase of the growth (when the critical threshold has been crossed) leads to the buckling of the membrane and the sheet is then only in partial contact with the container. Our results can be simply adapted to this closed problem. As expected we again find that there is a critical growth ϵ_{cr} above which the delamination is preferred with respect to the adhered solution. Indeed, the equations governing

the post-buckling behaviour are the same except for equation (2.10) that is to be replaced with

$$\pi r\epsilon = r\bar{\theta} + \frac{(1-\lambda)L}{2} + \lambda S.$$

It is worth noticing explicitly that even the energy expression (3.1) remains unchanged. By contrast, the adhered solution is characterized by a uniform stretch $\lambda_{\mathrm{adh}} = 1/(1+\epsilon)$ and its elastic energy is

$$W_{\mathrm{adh}} = \pi k r^{-1}(1+\epsilon)^{-1}(1+\epsilon^2\xi^{-2}).$$

However, it turns out that the two problems are mathematically equivalent provided we substitute $\Delta\alpha$ with $\pi\epsilon$. We finally find the following approximation for the critical growth: $\epsilon_{\mathrm{cr}} \approx 41.0912\,\xi^{6/5}$.

As an application of our results, we look at the experiment on the packing of flexible films reported in Boué *et al.* [2]. In the first part of their paper, the authors studied the pressure exerted by the sheet on the external container as a function of ϵ, here named *the confinement parameter*. Their experimental data exhibit an increasing pressure as the confinement parameter ϵ is decreased. Numerical studies of the elastica model indicate indeed a divergent pressure in the limit of $\epsilon \to 0$. This is also consistent with the theoretical results [13,14], which in addition show an asymptotic dependence of the internal forces, and hence the pressure, on $\epsilon^{-2/3}$. However, the thickness of the sheet used in the experiment is $h = 0.1$ mm, while the container radius is $r = 26$ mm. Since for a rectangular section $\ell = h/\sqrt{12}$, we obtain that $\xi = 1.11 \times 10^{-3}$ and $\epsilon_{\mathrm{cr}} = 1.17 \times 10^{-2}$. Unfortunately, the smallest experimental value of ϵ reported in figure 3 of Boué *et al.* [2] is just above this critical value and hence they are not able to see the transition experimentally. On the one hand, this justify the validity of the Elastica model above the critical threshold. On the other hand, our results predict that, by further decreasing ϵ, the hump should suddenly disappear. At the transition, the pressure (per unit length) on the container undergoes a jump to $P_{\mathrm{cr}} \approx br^{-1}\epsilon_{\mathrm{cr}}$, while below ϵ_{cr} the pressure is proportional to ϵ, hence it goes to zero as $\epsilon \to 0$. This solve the apparent paradox, described in Cerda & Mahadevan [13], De Pascalis *et al.* [14] and Boué *et al.* [2], of a diverging pressure in the low confinement regime.

In conclusion, the present analysis recognizes the key role played by stretchability for a correct description of the mechanical collapse of a loaded or growing elastic thin sheet adhered to a curved substrate. Even when the sheet is nearly unstretchable, the energetic contribution of compression cannot be neglected when the length scales in the problem are comparable with the sheet thickness (i.e. small humps). Our model yields analytic approximations for the critical threshold and the minimum size for the humps. This threshold depends on the reduced compressibility that, for homogeneous materials, is a purely geometrical dimensionless parameter. Furthermore, it sets an upper bound to the exerted pressure on the container. Future works can consider the effects of other physical quantities (i.e. capillary adhesion, intrinsic curvature and gravity) or the coupling of growth with internal stress [29] on the morphology and the critical parameters.

Data accessibility. No data associated with this work.

Authors' contributions. The authors contributed equally to this work.

Competing interests. We have no competing interests.

Funding. This research has been carried out within the Young Researchers Project 'Collasso Meccanico di Membrane Biologiche Confinate', supported by the Italian 'Gruppo Nazionale per la Fisica Matematica' (GNFM).

Acknowledgements. We wish to thank C. Morosi for helpful discussions. We also thank an anonymous referee for her/his suggestions, and in particular the recommendation to study the stability of the buckled solutions.

Appendix A. Variational formulation

In this section, we derive the first and the second variation of the energy functional of the collapsed solution. This energy consists of two parts: the energy of the detached region W_f and the energy of the adhered region W_{a}. The effective energy for the detached beam comprises the

bending energy, the compression energy and a term that enforces its endpoints to lie on the delimiting container:

$$W_f = \int_0^{\bar{S}} [k\theta'^2 + b(\lambda - 1)^2]\,\mathrm{d}S - 2T_x \left(r\sin\bar{\theta} + \int_0^{\bar{S}} \lambda\cos\theta\,\mathrm{d}S \right), \tag{A 1}$$

where T_x, that represents the horizontal component of the internal force, have the meaning of a Lagrange multiplier. Both T_x and $\bar{S}$ have to be determined in the minimization process.

In the adherent region, the sheet is in contact with the circular container and, therefore, the bending energy can be written as a function of the stretch. Furthermore, a geometrical constraint establishes an appropriate relation between the length of the adhered region and the other geometrical parameters of the problem,

$$\int_{\bar{S}}^{L/2} \lambda(S)\,\mathrm{d}S = \frac{L}{2} - r(\Delta\alpha - \bar{\theta}), \tag{A 2}$$

thus the effective energy for the adhered curve is

$$W_\mathrm{a} = \int_{\bar{S}}^{L/2} \left[k\frac{\lambda^2}{r^2} + b(\lambda - 1)^2 \right] \mathrm{d}S + 2\mu \left(\int_{\bar{S}}^{L/2} \lambda\,\mathrm{d}S - \frac{L}{2} + r(\Delta\alpha - \bar{\theta}) \right), \tag{A 3}$$

where μ is a Lagrange multiplier related to the constraint (A 2).

Let us introduce the varied quantities

$$\theta_\varepsilon(S) = \theta(S) + \varepsilon h(S) \quad \text{and} \quad \lambda_\varepsilon(S) = \lambda(S) + \varepsilon u(S). \tag{A 4}$$

The variational procedure must explicitly include the fact that the endpoints $S = 0$ and $S = L/2$ are fixed, while the detachment point $S = \bar{S}$ is not. We assume that $\theta_\varepsilon(\bar{S} + \varepsilon\delta\bar{S})$ and $\lambda_\varepsilon(\bar{S} + \varepsilon\delta\bar{S})$ are regular functions of ε. Therefore, each degree in their ε-expansion must agree when ε approaches zero from below or above, i.e. when $S \to \bar{S}^-$ or $S \to \bar{S}^+$. We thus obtain the following compatibility (or jump) conditions:

$$\theta(\bar{S}^-) = \theta(\bar{S}^+) = \bar{\theta}, \quad \lambda(\bar{S}^-) = \lambda(\bar{S}^+) = \bar{\lambda}, \tag{A 5a}$$

$$\theta'(\bar{S}^-)\delta\bar{S} + h(\bar{S}^-) = \theta'(\bar{S}^+)\delta\bar{S} + h(\bar{S}^+), \tag{A 5b}$$

$$\lambda'(\bar{S}^-)\delta\bar{S} + u(\bar{S}^-) = \lambda'(\bar{S}^+)\delta\bar{S} + u(\bar{S}^+) \tag{A 5c}$$

and

$$\tfrac{1}{2}\theta''(\bar{S}^-)\delta\bar{S} + h'(\bar{S}^-) = \tfrac{1}{2}\theta''(\bar{S}^+)\delta\bar{S} + h'(\bar{S}^+). \tag{A 5d}$$

(a) The first variation

The functional can be recast in the form

$$W = \int_0^{\bar{S}} w_f\,\mathrm{d}S + \int_{\bar{S}}^{L/2} W_\mathrm{a}\,\mathrm{d}S - 2T_x r\sin\bar{\theta} + 2\mu\left(-\frac{L}{2} + r(\Delta\alpha - \bar{\theta}) \right), \tag{A 6}$$

where $w_f := k(\theta')^2 + b(\lambda - 1)^2 - 2T_x\lambda\cos\theta$ and $W_\mathrm{a} := k\lambda^2/r^2 + b(\lambda - 1)^2 + 2\mu\lambda$. Thus, the first variation of W can be written as

$$\begin{aligned}\delta W = &\int_0^{\bar{S}} \left\{ \left[\frac{\partial w_f}{\partial\theta} - \left(\frac{\partial w_f}{\partial\theta'} \right)' \right] h + \frac{\partial w_f}{\partial\lambda} u \right\} \mathrm{d}S + \int_{\bar{S}}^{L/2} \frac{\partial W_\mathrm{a}}{\partial\lambda} u\,\mathrm{d}S \\ &+ \left(\frac{\partial w_f}{\partial\theta'} \right)_{S=\bar{S}} h(S^-) - 2\mu r h(S^+) + (w_f - W_\mathrm{a} - 2rT_x\theta'\cos\theta)_{S=\bar{S}}\delta\bar{S}.\end{aligned} \tag{A 7}$$

The request that the first term of (A 7) vanishes for any arbitrary choice of $h(S)$ and $u(S)$, leads to equilibrium equations (2.5) and (2.6) for the buckled part of the beam. On the other hand, the

vanishing of the second integral of (A 7) for any $u(S)$ yields the equation

$$k\frac{\lambda}{r^2} + b(\lambda - 1) + \mu = 0, \tag{A 8}$$

whence we deduce that λ is constant in the adhered part. The Lagrange multiplier μ is then determined from (A 2), which reduces to (2.10) if $\lambda = \bar{\lambda}$. Finally, we set $h(\bar{S}^+) = 0$ and $\theta'(\bar{S}^+) = -\bar{\lambda}/r$ in (A 5) so that the compatibility conditions can be used to simplify the boundary terms of (A 7) to

$$-\frac{k}{r^2}(\bar{\lambda} + r\theta'(\bar{S}^-))^2\delta\bar{S}, \tag{A 9}$$

which yields the transversality conditions (2.8). Thus, in agreement with the first Weierstrass–Erdmann condition, $\theta'(S)$ is continuous in $S = \bar{S}$.

(b) The second variation

Before embarking on the calculation of the second variation, we first need to establish some identities in order to be able to simplify the final expression. The geometrical constraint (2.9) must be satisfied also by the varied configurations. To first order in ε this implies

$$\int_0^{\bar{S}} (\cos\theta^* u - \lambda^* \sin\theta^* h)\,\mathrm{d}S = 0, \tag{A 10}$$

where $\theta^*(S)$ and $\lambda^*(S)$ are the equilibrium solutions and we have used the (first order) compatibility conditions (A 5) and the continuity of $\theta'(S)$.

The second-order conditions (A 5), which are needed for the second variations, can be simplified by assuming $h'(\bar{S}^+) = 0$, $\theta''(\bar{S}^+) = 0$ and $\theta''(\bar{S}^-) = -\bar{\lambda}\tau\sin\bar{\theta}$ where this last identity comes from the equilibrium equation (2.6). We are now ready to calculate the second variation of the free part which, after some algebraic manipulations, can be written as

$$\delta^2 W_f = 2k\int_0^{\bar{S}} \left[(h')^2 - \tau h(\lambda^*\cos\theta^* h + 2\sin\theta^* u) + \frac{b}{k}u^2\right]\mathrm{d}S. \tag{A 11}$$

The second variation of the functional related to the adhered part is

$$\delta^2 W_\mathrm{a} = 2\frac{k + br^2}{r^2}\int_{\bar{S}}^{L/2} u^2\,\mathrm{d}S. \tag{A 12}$$

This is positive definite and can always be set to zero by choosing $u(S) \equiv 0$ in $S \in (\bar{S}, L/2)$ so that its contribution to the stability of the system can be neglected.

References

1. Sakashita A, Imai M, Noguchi H. 2014 Morphological variation of a lipid vesicle confined in a spherical vesicle. *Phys. Rev. E* **89**, 040701. (doi:10.1103/PhysRevE.89.040701)
2. Boué L, Adda-Bedia M, Boudaoud A, Cassani D, Couder Y, Eddi A, Trejo M. 2006 Spiral patterns in the packing of flexible structures. *Phys. Rev. Lett.* **97**, 166104. (doi:10.1103/PhysRevLett.97.166104)
3. Vella D, Bico J, Boudaoud A, Roman B, Reis PM. 2009 The macroscopic delamination of thin films from elastic substrates. *Proc. Natl Acad. Sci. USA* **106**, 10 901–10 906. (doi:10.1073/pnas.0902160106)
4. Wagner TJW, Vella D. 2013 The 'sticky elastica': delamination blisters beyond small deformations. *Soft Matter* **9**, 1025–1030. (doi:10.1039/C2SM26916C)
5. Sun Y, Choi WM, Jiang H, Huang YY, Rogers JA. 2006 Controlled buckling of semiconductor nanoribbons for stretchable electronics. *Nat. Nanotechnol.* **1**, 201–207. (doi:10.1038/nnano.2006.131)
6. Boulogne F, Giorgiutti-Dauphiné F, Pauchard L. 2013 The buckling and invagination process during consolidation of colloidal droplets. *Soft Matter* **9**, 750–757. (doi:10.1039/C2SM26530C)

7. Fargette A, Neukirch S, Antkowiak A. 2014 Elastocapillary snapping: capillarity induces snap-through instabilities in small elastic beams. *Phys. Rev. Lett.* **112**, 137802. (doi:10.1103/PhysRevLett.112.137802)
8. Omara A, Guice L, Straughan W, Akl F. 1997 Buckling models of thin circular pipes encased in rigid cavity. *J. Eng. Mech. ASCE* **123**, 1294–1301. (doi:10.1061/(ASCE)0733-9399(1997)123:12(1294))
9. Vasilikis D, Karamanos SA. 2009 Stability of confined thin-walled steel cylinders under external pressure. *Int. J. Mech. Sci.* **51**, 21–32. (doi:10.1016/j.ijmecsci.2008.11.006)
10. Holland MA, Kosmata T, Goriely A, Kuhl E. 2013 On the mechanics of thin films and growing surfaces. *Math. Mech. Solids* **18**, 561–575. (doi:10.1177/1081286513485776)
11. Goriely A *et al.* 2015 Mechanics of the brain: perspectives, challenges, and opportunities. *Biomech. Model. Mechanobiol.* **14**, 931–965. (doi:10.1007/S10237-015-0662-4)
12. Dodwell TJ, Hunt GW, Peletier MA, Budd CJ. 2012 Multi-layered folding with voids. *Phil. Trans. R. Soc. A* **370**, 1740–1758. (doi:10.1098/rsta.2011.0340)
13. Cerda E, Mahadevan L. 2005 Confined developable elastic surfaces: cylinders, cones and the elastica. *Proc. R. Soc. A* **461**, 671–700. (doi:10.1098/rspa.2004.1371)
14. De Pascalis R, Napoli G, Turzi SS. 2014 Growth-induced blisters in a circular tube. *Phys. D* **283**, 1–9. (doi:10.1016/j.physd.2014.05.008)
15. Rim JE, Purohit PK, Klug WS. 2014 Mechanical collapse of confined fluid membrane vesicles. *Biomech. Model. Mech.* **13**, 1277–1288. (doi:10.1007/s10237-014-0572-x)
16. Kahraman O, Stoop N, Müller MM. 2012 Morphogenesis of membrane invaginations in spherical confinement. *EPL* **97**, 68008. (doi:10.1209/0295-5075/97/68008)
17. Rayleigh JWS. 1877 *The theory of sound*. London, UK: Macmillan and Co.
18. Magnusson A, Ristinmaa M, Ljung C. 2001 Behaviour of the extensible elastica solution. *Int. J. Solids Struct.* **38**, 8441–8457. (doi:10.1016/S0020-7683(01)00089-0)
19. Audoly B, Pomeau Y. 2010 *Elasticity and geometry: from hair curls to the non-linear response of shells*. Oxford, UK: Oxford University Press.
20. Pauchard L, Rica S. 1998 Contact and compression of elastic spherical shells: the physics of a 'ping-pong' ball. *Phil. Mag. B* **78**, 225–233. (doi:10.1080/13642819808202945)
21. Pandey A, Moulton DE, Vella D, Holmes DP. 2014 Dynamics of snapping beams and jumping poppers. *Europhys. Lett.* **105**, 24001. (doi:10.1209/0295-5075/105/24001)
22. Lee AA Gouellec CL, Vella D. 2015 The role of extensibility in the birth of a ruck in a rug. (http://arxiv.org/abs/1508.05380)
23. Dill EH. 1992 Kirchhoff's theory of rods. *Arch. Hist. Exact. Sci.* **44**, 1–23. (doi:10.1007/BF00379680)
24. Abramowitz M, Stegun IA. 1964 *Handbook of mathematical function with formulas, graphs, and mathematical tables*. New York, NY: Dover.
25. Gelfand IM, Fomin SV. 1963 *Calculus of variations*. Englewood Cliffs, NJ: Prentice-Hall.
26. van Brunt B. 2004 *The calculus of variations*. New York, NY: Springer.
27. Manning RS, Rogers KA, Maddocks JH. 1998 Isoperimetric conjugate points with application to the stability of DNA minicircles. *Proc. R. Soc. Lond. A* **454**, 3047–3074. (doi:10.1098/rspa.1998.0291)
28. Hoffman KA, Manning RS, Paffenroth RC. 2002 Calculation of the stability index in parameter-dependent calculus of variations problems: buckling of a twisted elastic strut. *SIAM J. Appl. Dyn. Syst.* **1**, 115–145. (doi:10.1137/S1111111101396622)
29. Tiero A, Tomassetti G. In press. On morphoelastic rods. *Math. Mech. Solids* (doi:10.1177/1081286514546178)